Earth and Planetary Science Letters 512 (2019) 227–235

Contents lists available at ScienceDirect

Earth and Planetary Science Letters

www.elsevier.com/locate/epsl

# An abrupt decrease in Southern Hemisphere terrestrial temperature during the Eocene–Oligocene transition

David Auerbach Colwyn [a,*,1], Michael T. Hren [b,c]

[a] Department of Geology and Geophysics, Yale University, New Haven, CT, USA
[b] Center for Integrative Geosciences, University of Connecticut, Storrs, CT, USA
[c] Department of Chemistry, University of Connecticut, Storrs, CT, USA

ARTICLE INFO

*Article history:*
Received 11 March 2018
Received in revised form 25 January 2019
Accepted 31 January 2019
Available online xxxx
Editor: J. Adkins

*Keywords:*
Eocene–Oligocene transition
terrestrial paleoclimate
precipitation stable isotopes
paleotemperature
Patagonia

ABSTRACT

Earth's climate transitioned from the greenhouse conditions of the Eocene to the icehouse of the Oligocene ~34 million years ago. Global cooling was triggered by a decrease in atmospheric $pCO_2$ and is associated with the first appearance of large, permanent ice-sheets on Antarctica. The Eocene–Oligocene transition (EOT) is marked by a large two-step increase in the $\delta^{18}O$ of benthic foraminifera, reflecting a combination of cooler global temperatures and continental ice growth. We measured the hydrogen isotope composition of hydrated volcanic glasses deposited in Patagonia during the EOT to reconstruct stable isotope hydrology and associated changes in temperature during this critical climate transition. These data show changes in stable hydrogen isotope ratios that are consistent with Patagonian terrestrial mean annual temperature decreasing by ~5 °C during the EOT before returning to 2 °C below pre-EOT values by the Early Oligocene. This is approximately synchronous with Northern Hemisphere cooling during the EOT, and indicates close coupling of temperature and atmospheric $pCO_2$.



## 1. Introduction

The abrupt shift of global climate from the ice-free greenhouse climate of the Late Eocene (Pearson et al., 2007) to the icehouse climate of the Early Oligocene (Galeotti et al., 2016) is perhaps the most dramatic climate transition of the Cenozoic. The transition between climate states occurs at the end of a cooling trend in the Late Eocene, following which temperature fluctuated before settling into a stable cool temperature regime by ~32 Ma (e.g., Lear et al., 2008). This change in climate state is marked by a rise in the $\delta^{18}O$ of benthic foraminifera (Zachos et al., 2001). While the onset of Antarctic glaciation (Galeotti et al., 2016) has been attributed to the opening of ocean gateways and thermal isolation of Antarctica (Kennett, 1977), coupled climate and ice sheet models show that it was far more likely a result of long-term decreases in atmospheric $pCO_2$ (DeConto and Pollard, 2003; Goldner et al., 2014). These models predict that the transition from ice-free to ice-present conditions should have been rapid and occurred in two steps. This two-step transition is documented in the $\delta^{18}O$ of well-preserved benthic foraminifera (Coxall et al., 2005; Lear et al., 2008) and $\varepsilon_{Nd}$ estimates of Antarctic weathering (Scher et al., 2011), and is contemporaneous with the timing of falling atmospheric $pCO_2$ (Pagani et al., 2005; Pearson et al., 2009; Zhang et al., 2013).

However, the terrestrial record of the EOT is less clear. This is due to the fact that in the terrestrial realm, high-quality age control is often lacking and sedimentation may be more intermittent in nature than in deep water marine settings. Records of the EOT in the Northern Hemisphere are marked by regionally variable changes in hydrology and temperature (Hren et al., 2013; Sheldon, 2009; Sheldon et al., 2012, 2016; Terry, 2001; Zanazzi et al., 2007), although most show cooling in the range of 4–8 °C (Hren et al., 2013; Zanazzi et al., 2007) from the Late Eocene to Early Oligocene. In contrast, the only terrestrial records of the EOT in the Southern Hemisphere come from Australia (Korasidis et al., 2018) and Patagonia, where phytoliths (Dunn et al., 2015; Strömberg et al., 2013) and $\delta^{18}O$ of tooth enamel and soil carbonate (Kohn et al., 2004, 2015) have been interpreted to show no change in climate across the EOT. The only large change observed in Patagonia during this period is a transient shift in the delivery of dust and suppression of wildfire associated with the earliest Oligocene glacial maximum (EOGM) (Selkin et al., 2015). A lack of observed cooling in Patagonia across the EOT is particularly

* Corresponding author at: Department of Geology and Geophysics, Yale University, P.O. Box 208109, New Haven, CT 06520-8109, USA.
*E-mail address:* david.colwyn@colorado.edu (D.A. Colwyn).
[1] Present address: Department of Geological Sciences, University of Colorado-

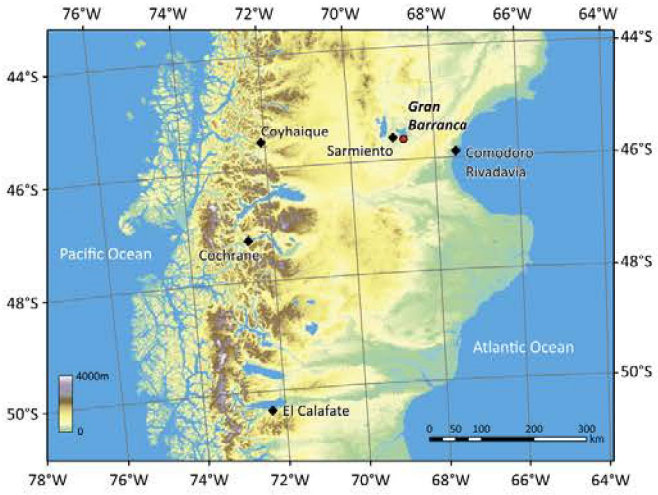


**Fig. 1.** Topography of central Patagonia at 1:4,000,000 scale. The location of the Gran Barranca section is indicated by the red circle; black diamonds identify regional cities of note. (For interpretation of the colors in the figure(s), the reader is referred to the web version of this article.)

boring Antarctica through this interval (Galeotti et al., 2016), as well as marine $U^{37}_{K'}$ and $TEX_{86}$ surface temperature data from DSDP Site 511 on the Falkland Plateau adjacent to eastern Patagonia (Liu et al., 2009) that show a large decrease in sea surface temperature (SST) during the EOT. The interpretation of a static climate in Patagonia during the EOT therefore challenges our understanding of ocean–atmosphere connectivity. Here we present a new high-resolution record of stable hydrogen isotopes ($\delta$D) from volcanic glass deposited in South America (~46°S) during this critical transition. Stable isotopes of precipitation are, to first order, controlled by temperature, and thus provide way to quantify regional climatic change during the EOT. These new data address the apparent dichotomy between hemispheres, and indicate a significant isotopic and climatic response to falling atmospheric $pCO_2$ similar to that observed in the Northern Hemisphere.

## 2. Geologic setting

We collected 23 volcanic ash samples from the Sarmiento Formation (Ameghino, 1889, 1906; Bellosi, 2010b; Madden et al., 2010; Simpson, 1930) at Gran Barranca in Chubut, Argentina (Fig. 1) to develop a new hydrogen isotope record of hydration water in ancient volcanic glass. The stratigraphic section at Gran Barranca is remarkable in its exceptional degree of stratigraphic completeness and highly resolved geochronological constraints (Dunn et al., 2013; Ré et al., 2010a, 2010b). The Eocene–Miocene Sarmiento Formation contains six members, including the valley-filling Eocene–Oligocene Vera Member. The Vera Member represents relatively uninterrupted deposition, showing poor soil development and no evidence of internal discontinuities (Bellosi, 2010a). This unit is composed primarily of felsic wind-transported volcanic material that was deposited following eruptions of the Andean volcanic arc to the west (Bellosi, 2010a) (Fig. 2). We sampled a continuous stratigraphic profile at Profile K, one of the thickest exposures of the Vera Member (Bellosi, 2010b). The high sedimentation rates in the Vera Member enabled sampling across the EOT with ca. 25 kyr resolution. All sample heights were referenced to the measured section and dated volcanic tuffs (Dunn et al., 2013; Ré et al., 2010a) in the Vera Member and the Lower and Upper Puesto Almendra Members. While the Vera Member lies stratigraphically between the Lower and Upper Puesto Almendra Members, it is not physically between them in outcrop due to the valley-filling nature of the Vera. Age control is provided by zircon U/Pb geochronology on volcanic tuffs (Dunn et al., 2013) and magnetostratigraphy (Ré et al., 2010b) (Fig. 2).

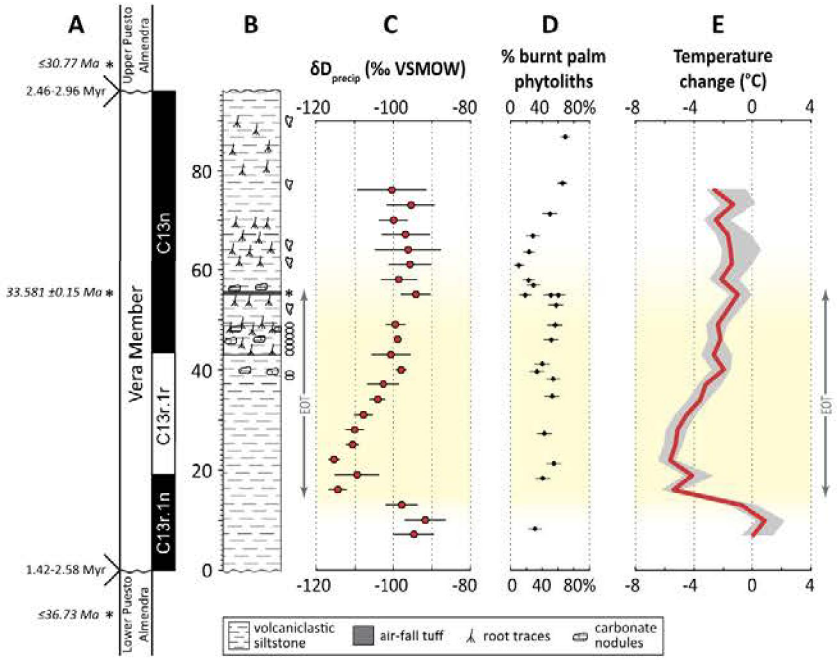


**Fig. 2.** Stratigraphy and geochemistry of studied sedimentary section of the Vera Member of the Sarmiento Formation (Bellosi, 2010b). (**A**) Radiometric (Dunn et al., 2013), lithostratigraphic (Bellosi, 2010b), and magnetostratigraphic (Dunn et al., 2013; Ré et al., 2010b) framework for the Vera Member. Radiometric dates indicated by asterisks

## 3. Hydration of volcanic glass

Reconstructing ancient stable isotopes of precipitation requires a material that samples the stable isotope chemistry of precipitation during formation and then remains stable over geologic timescales. We measured $\delta$D of volcanic glass preserved in the Vera Member to reconstruct the isotopic composition of precipitation through time. During volcanic eruptions, magma degasses and forms glass fragments, which typically retain 0.1–0.3 wt. % of magmatic water (Friedman and Smith, 1958; Martin et al., 2017; Ross and Smith, 1955). These glasses are then hydrated by meteoric water, which saturates at up to 6 wt. % water (Friedman et al., 1993a; Cassel and Breecker, 2017). Glass hydration occurs over 1–10 kyr (Cassel et al., 2009; Friedman et al., 1993b; Seligman et al., 2016), and is rapid compared to timescales of climate change during the Late Eocene to Early Oligocene. During the saturation process, alkali cations (e.g., $Na^+$, $K^+$) are exchanged for $H^+$ from the meteoric water (Cerling et al., 1985; Cassel and Breecker, 2017). As this exchange occurs, the rim of the glass particle becomes impermeable to further diffusion of water (Friedman and Long, 1976) and thus glass particles do not undergo significant further isotopic exchange with the environment (Friedman and Long, 1984). Preservation of glass in and of itself attests to the fact that ancient sedimentary environments in which glass is found did not allow sufficient fluid availability to allow complete conversion of glass to secondary clays. Following hydration, the resulting glass particles effectively preserve a record of the time-averaged $\delta$D of precipitation during hydration (Dettinger and Quade, 2015; Friedman et al., 1993b; Seligman et al., 2016).

## 4. Materials and methods

Fresh rock samples were collected from felsic volcaniclastic sediments of aeolian origin (Bellosi, 2010a) in the measured sedimentary section (Fig. 2). We separated volcanic glasses from clays and other hydrous minerals using established mineral separation procedures. Rock samples were crushed with a mortar and pestle and then sieved to a 63–180 µm fraction. The sieved fraction was agitated in deionized water and left to settle until particles >63 µm had settled; the remaining clay-rich liquid was decanted. This was repeated 3–5 times, depending on the concentration of clay particles. Samples were then placed in a sonicating bath with sodium pyrophosphate deflocculant for 10 min in order to remove any clay particles adhering to grain surfaces. Following sonication, the samples were agitated in a 10% HCl solution to remove any carbonate. Samples were then rinsed repeatedly and dried at 40 °C. Magnetic grains were separated using repeated runs through a Frantz magnetic separator at progressively increasing magnet strengths. Resulting non-magnetic separates were density-separated using lithium polytungstate heavy liquid and then inspected using a microscope to determine the purity of glass separates. A subset of samples was inspected using SEM to confirm their preservation and the lack of significant secondary hydrous minerals (Fig. 3).

High-purity samples were weighed into silver capsules, stored in a desiccating jar, and then dried in a vacuum oven at 80 °C for 24 h prior to analysis. Drying at higher temperature and longer time produces essentially identical $\delta$D and water contents (Fig. S1). The $\delta$D of glass separates was measured using a thermal conversion elemental analyzer (TC/EA) attached to a Thermo MAT 253 IRMS at the University of Connecticut. Isotopic compositions of relative to VSMOW and errors reflect standard deviation of multiple analyses. The $\delta$D of the most repeated standards was PEF-1 = $-102 \pm 2$‰, NBS-22 = $-118 \pm 2$‰, and KGa-1b = $-65 \pm 2$‰. The known water content of NBS-22 was used to calculate water contents of glasses. Measured $\delta$D of glass was used to calculate the $\delta$D of hydration water (precipitation) using the fractionation factor of Friedman et al. (1993a), which has been replicated in recent studies (Seligman et al., 2016; Porter et al., 2016). During interpretation, we assumed that any remnant magmatic water had a negligible effect on the measured $\delta$D because (1) the $\delta$D of nearby degassed rhyolite (Castro et al., 2014) is similar to the range of values we observe and (2) magmatic water is likely to have undergone complete isotopic exchange with hydration water in glasses of Eocene–Oligocene age.

## 5. Results and age models

The Vera Member is known to span a time interval of ~0.7 to ~2.0 Myr that includes the EOT (Dunn et al., 2013). During this time, the $\delta$D of volcanic glasses in the Vera Member abruptly decreases from $-125 \pm 3$‰ to $-142 \pm 3$‰ and then recovers more gradually between 10 and 40 m in the section to nearly pre-excursion values of $-128 \pm 2$‰ (Fig. 2, Table 1). To place this geochemical excursion into a time framework, we use the depositional age model of Dunn et al. (2013), which integrates the available radiometric ages and magnetostratigraphy. Their age model for the Vera Member includes the 33.581±0.15 Ma La Cancha tuff (Fig. 2), as well as radiometric constraints from the Lower Puesto Amendra Member and Upper Puesto Almendra Member, which, respectively, lie stratigraphically below and above the Vera Member (Dunn et al., 2013; see Fig. 2). The preferred age model of Dunn et al. (2013) correlates the reversed magnetic polarity interval in the lowest part of the Vera Member with chron C13r.1n. The existence of 'cryptochron' C13r.1 is well established (Channell et al., 2003), and we follow this interpretation for the age model of the Vera Member. This indicates that the abrupt $\delta$D decrease occurs at ~34.2 Ma, followed by the slower recovery between ~34.0 and ~33.5 Ma (Table 1). This chronology is generally consistent with other records of the timing of change associated with the EOT elsewhere on land and in the ocean (e.g., Coxall et al., 2005; Hren et al., 2013; Lear et al., 2008).

## 6. Precipitation stable isotopes and temperature

The hydrogen isotopic composition of volcanic glass within the Vera Member records a decrease of ~20‰ during the time period associated with the EOT. This indicates a significant change in the isotopic composition of ambient water in the region during this transition period. There are a number of factors that influence the isotopic composition of water in South America, including changes in atmospheric circulation (e.g., Hoke et al., 2013; Liu et al., 2010) and topography (e.g., Poage and Chamberlain, 2001). However, globally and locally, stable isotopes of precipitation have a clear observed relationship with temperature at mid and high latitudes (Bowen and Wilkinson, 2002; Dansgaard, 1964; Rozanski et al., 1993) due to temperature-dependent fractionation that occurs during (1) evaporation from the source and (2) partitioning between vapor and precipitation during rainout (e.g., Bowen and Revenaugh, 2003; Gat, 1996). More specifically, the net fractionation of stable isotopes reflects the difference between the temperature at which this partitioning occurs (Pierrehumbert,

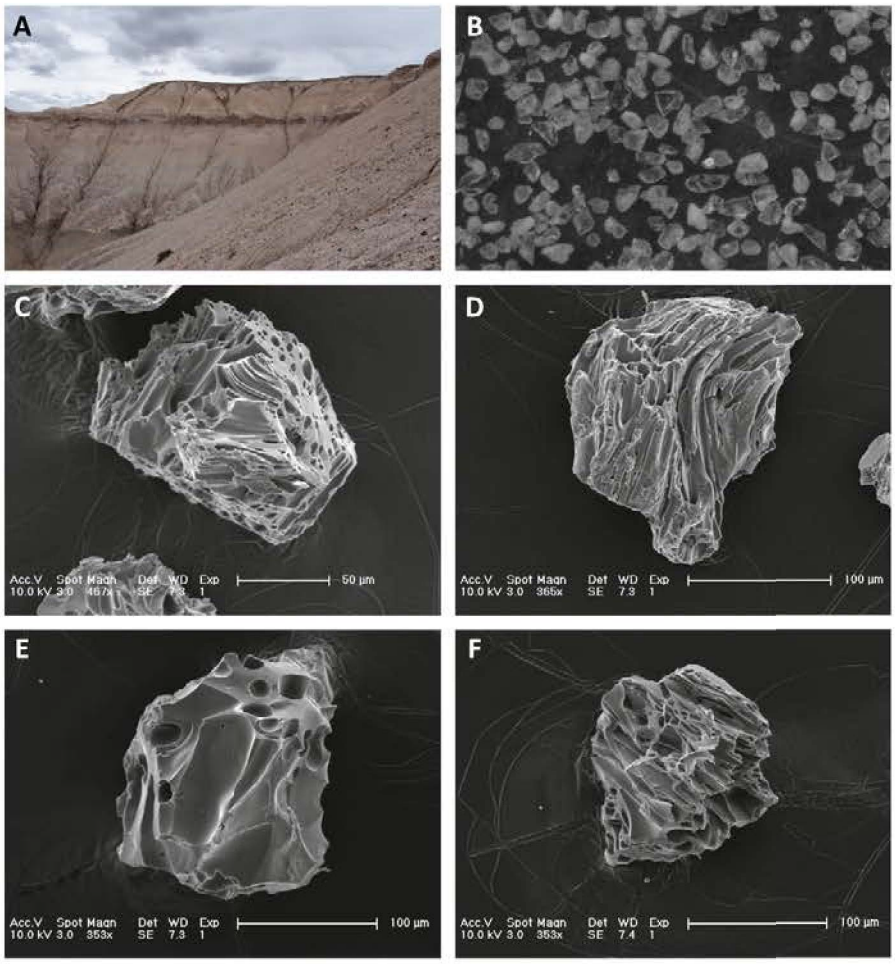


**Fig. 3.** (**A**) Field photo of the Vera Member at Gran Barranca, near Profile K. (**B**) Light microscope view of typical volcanic glass separate. 2.5X magnification, field of view is 3 mm across. (**C–F**) Scanning electron microscope images of Vera Member glass separates from samples 13GB13, 13GB17, 13GB23, and 13GB25, respectively. Images show primary volcanic textures and sharp edges, as well as minimal secondary clay particles on grain surfaces.

**Table 1**
Measured $\delta D$ of volcanic glasses in the Vera Member, Sarmiento Formation, and reconstructed meteoric water values.

| Sample | Stratigraphic height (m) | Model age (Ma) | $\delta D_{glass}$[a] (‰ VSMOW) | $N$ | $2\sigma$ error | $H_2O$ (wt. %) | $\delta D_{water}$[b] (‰ VSMOW) |
|---|---|---|---|---|---|---|---|
| 13GB12 | 7 | 34.331 | −125 | 3 | 5.4 | 0.7% | −95 |
| 13GB13 | 10 | 34.284 | −122 | 2 | 1.7 | 4.3% | −92 |
| 13GB14 | 13 | 34.237 | −128 | 3 | 4.1 | 0.6% | −98 |
| 13GB15 | 16 | 34.190 | −144 | 3 | 1.9 | 1.0% | −114 |
| 13GB16 | 19 | 34.085 | −139 | 2 | 5.8 | 4.1% | −110 |
| 13GB17 | 22 | 34.038 | −145 | 3 | 1.5 | 0.9% | −115 |
| 13GB18 | 25 | 33.990 | −140 | 3 | 1.7 | 0.8% | −111 |
| 13GB19 | 28 | 33.943 | −139 | 3 | 2.5 | 0.6% | −110 |
| 13GB20 | 31 | 33.895 | −137 | 3 | 2.4 | 0.7% | −108 |
| 13GB21 | 34 | 33.848 | −134 | 3 | 2.1 | 0.8% | −104 |
| 13GB22 | 37 | 33.800 | −132 | 2 | 4.2 | 6.1% | −103 |
| 13GB23 | 40 | 33.753 | −128 | 3 | 1.4 | 0.7% | −98 |
| 13GB25 | 43 | 33.705 | −130 | 3 | 4.6 | 0.6% | −101 |
| 13GB26 | 46 | 33.674 | −129 | 3 | 0.6 | 0.7% | −99 |
| 13GB28 | 49 | 33.643 | −129 | 3 | 2.6 | 0.7% | −99 |
| 13GB32 | 55 | 33.581 | −124 | 2 | 3.7 | 4.9% | −94 |
| 13GB33 | 58 | 33.571 | −128 | 3 | 4.8 | 0.8% | −99 |
| 13GB34 | 61 | 33.560 | −126 | 3 | 5.6 | 0.7% | −96 |
| 13GB35 | 64 | 33.550 | −126 | 2 | 5.1 | 2.6% | −96 |
| 13GB36 | 67 | 33.539 | −127 | 3 | 6.3 | 0.5% | −97 |
| 13GB37 | 70 | 33.529 | −130 | 3 | 3.8 | 0.5% | −100 |
| 13GB38 | 73 | 33.518 | −125 | 3 | 6.3 | 0.5% | −95 |

records requires an assessment of the potential effects of temperature change on isotopic composition as well as factors such as changes in water source or mixing of air masses.

Gran Barranca is situated approximately 150 km from the Atlantic Ocean to the east and less than 500 km from the Pacific to the west at ~45°S latitude. Over the relatively short time interval represented in the Vera Member sediments, it is not geologically plausible for the latitudinal position of Patagonia, the distance of Gran Barranca from vapor sources in the Pacific Ocean, or the height of the Andes to have changed significantly. Precipitation in Patagonia is fed by water vapor carried by the Southern Hemisphere westerly wind belt (SWWB) (Garreaud et al., 2009), although minor mixing with vapor from Atlantic can occur near the east coast (Garreaud et al., 2013). The position and direction of the SWWB results from the speed and direction of Earth's rotation (Schneider, 2006; Williams, 1988), which has changed little over the Cenozoic (Parrish et al., 1982). Thus we consider the SWWB a persistent feature of global and Patagonian climate. While the SWWB has been observed to shift north and south by several degrees of latitude in response to changes in global climate (Koffman et al., 2014; Lamy et al., 2001; Moy et al., 2008), volcanic ash dispersal patterns confirm that Patagonia has remained within the band of westerly winds throughout the Cenozoic (Bellosi, 2010a; Rapela et al., 1988). Wind strength might have changed over the Cenozoic, although the pattern of westerly circulation did not. Consequently, changes in moisture source are not a significant factor in determining precipitation $\delta$D over geologic time scales in Patagonia. We also infer that evaporation had little to no effect on the $\delta$D of meteoric water during both precipitation and storage, based on modern observations of precipitation $\delta$D (Smith and Evans, 2007; Stern and Blisniuk, 2002) and the sedimentary facies present at Gran Barranca (Bellosi, 2010a, 2010b; Bellosi and Gonzalez, 2010), respectively.

Over short time scales (hours to years), $\delta$D of precipitation can be highly variable (e.g., Coplen et al., 2008), but values collapse around a mean at decadal or longer timescales (Liu et al., 2010). Thus, records that integrate precipitation $\delta$D over long time scales preserve such a time-averaged value. Because volcanic glass hydrates over 1–10 kyr (Friedman and Long, 1976), it thus records averages of precipitation over those millennial timescales. Conversely, it also means that variation on shorter-than-kyr timescales—synoptic events and shorter-term variation such as ENSO and the sunspot cycle—does not appear in the record.

Because the mid-latitude climate of Patagonia minimizes non-temperature effects on hydrogen isotopes of precipitation, we use modern hydrogen isotope and temperature data from IAEA-GNIP stations in Patagonia to quantify the relationship between regional temperature and precipitation $\delta$D. This approach that has been previously utilized to reconstruct Cenozoic temperatures in this region (Kohn et al., 2004) and specifically includes seasonal data that is known to reflect the range of potential variability in moisture source. We selected four low-elevation stations across Patagonia with relatively long precipitation stable isotope records: Bariloche (−41.15°S, −71.33°W, records span 1996–2002), Puerto Montt (−41.47°S, −72.93°W, 1964–2014), Coyhaique (−45.35°S, −72.07°W, 1988–1999), and Punta Arenas (−53.0°S, −70.51°W, 1990–2014). These sites span a range of modern climatic conditions, including wind speed, MAT, and precipitation amount. Data from each station was averaged monthly, which is reported in Table S1.

All sites show a strong linear relationship ($r^2$ ranges from 0.70

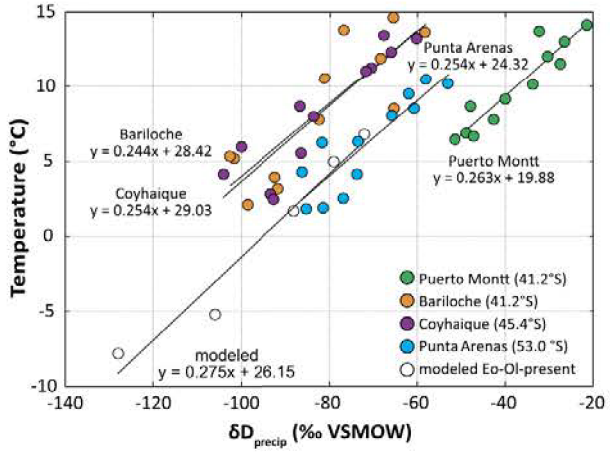


**Fig. 4.** $\delta$D–temperature relationships for IAEA-GNIP stations across Patagonia and isotope-enabled GCM data for the geologic past, including the time around the EOT (Feakins et al., 2014). Note the consistent slope of modern and ancient relationships in Patagonia.

temperature across space and short timescales and demonstrates that, independent of season, all southern Patagonia sites reflect the same dependence of stable hydrogen isotopes on temperature. A regional mean relationship was calculated from the entire data set, yielding a single equation that relates regional temperature to stable hydrogen isotope ratio: $T$ (°C) = 0.254 ($\delta$D) + 25.41. As a conservative approach, we use the stations with the steepest $\delta$D–$T$ slopes (Puerto Montt, $y = 0.263x + 19.88$) and shallowest (Bariloche, $y = 0.244x + 28.42$) as end members that describe the entire range of potential climate variation due to latitudinal shifts in climate belts and ocean temperature change. These regressions were then applied to the reconstructed precipitation $\delta$D from the Vera Member to estimate the mean and possible range of temperature change during the EOT (Fig. 2). Importantly, we base our interpretations on the *relative* change in $\delta$D, which can be effectively reconstructed in the geologic past using the slope of the $\delta$D–$T$ relationship.

While GNIP observations support the use of this $\delta$D–$T$ relationship across space and short time scales, some model predictions indicate that the slope of the $\delta$–$T$ relationship for northern hemisphere sites during warm periods in the geologic past may be shallower than modern (Fricke and O'Neil, 1999; Jouzel et al., 1997; Kohn et al., 2004; Secord et al., 2010). However, a comparison of modern GNIP data against modeled MAT and $\delta$D data for the southern hemisphere during the late Eocene to early Oligocene shows a similar $\delta$–$T$ relationship to the modern. Feakins et al. (2014) used an isotope-enabled GCM to simulate climate on the nearby Antarctic Peninsula for the late Eocene, Eocene–Oligocene transition, early and late Oligocene, and present. A regression through these data yields nearly the same slope as the modern GNIP data (Fig. 4). The decision to use a modern $\delta$–$T$ slope to reconstruct the past temperatures in Patagonia is supported by the agreement of modern observations with reconstructed slopes for the mid-latitudes in the geologic past (Kohn et al., 2004; Secord et al., 2010) and the observation that Patagonia has remained at approximately its modern latitude through the Cenozoic (Seton et al., 2012). In addition, model predictions for the precipitation stable isotope response for Patagonia from the late Eocene to early Oligocene (Feakins et al., 2014) are comparable to the magnitude of change that we observe. Agreement between modeled ancient

ancient, including vapor source, atmospheric circulation patterns, topography, convection, and continentality (Charles et al., 1994; Schmidt et al., 2007). While the use of the modern observed relationship in the geologic past of Patagonia appears justified, care should be used when applying this approach to other regions in deep time.

Using the observed $\delta D$–$T$ relationship, we reconstruct regional terrestrial temperature from the glass $\delta D$, taking into account the effect of stepwise changes in ice volume during the EOT (Bohaty et al., 2012) on source composition. To do this, we assume instantaneous ice growth and apply a correction of 0.6‰ in $\delta^{18}O$, or 4.8‰ $\delta D$. Following existing work on the effect of ice growth on marine $\delta^{18}O$ (Bohaty et al., 2012; Lear et al., 2008), we apply a decrease in $\delta^{18}O$ of 0.2‰ at the first step in the benthic foraminiferal record (16 m in our measured section) and a decrease of 0.4‰ at the second step (25 m in our section). While we acknowledge this does not likely reflect the true complexity of the pacing of ice volume growth, this approach provides a conservative treatment of the data. Modern precipitation stable isotope data and GCM simulations of Eocene to Oligocene precipitation stable isotopes for the nearby Antarctic Peninsula (Feakins et al., 2014) predict that for every 1 °C change in temperature, the $\delta D$ of precipitation should change on the order of ~4‰ or more. The rapid decrease in glass and meteoric $\delta D$ observed in the Vera Member at Gran Barranca indicates a rapid cooling of $\sim 5 \pm 1$ °C (range reflects uncertainty in the $\delta D$–$T$ relationship) during the onset of the EOT (Fig. 5). By ~33.5 Ma (above the 33.581 Ma La Cancha Tuff), temperatures return to approximately −2 °C relative to pre-EOT values (Fig. 5). The initial fall in temperature is coincident with the onset of the $\delta^{18}O$ shift in the marine benthic foraminifera record (Fig. 5), and the recovery occurs over ~600 kyr. Unlike marine records, terrestrial records did not suffer from carbonate dissolution (e.g., Coxall et al., 2005), thus the Vera Member may capture an interval of time typically missing from marine records of the EOT (albeit at much lower resolution).

A cooling of ~5 °C on land in Patagonia matches well with the temperature change observed during the EOT in Northern Hemisphere records (Hren et al., 2013; Zanazzi et al., 2007). In addition, this magnitude of change is identical to the modeled and observed magnitude of change in SST at high latitude marine sites, including DSDP Site 511 located on the nearby Falklands Plateau (Liu et al., 2009). While changes in hydrology appear to be heavily dependent on the regional setting, differing even in sign (Hren et al., 2013; Sheldon, 2009), the terrestrial cooling signal appears to be a common characteristic of Northern Hemisphere EOT records. Our observation that such cooling also occurred in the Southern Hemisphere emphasizes the global and at least broadly synchronous nature of the terrestrial climate response to the EOT.

## 7. Discussion

High latitude terrestrial cooling in South America was broadly synchronous with the initiation of cooling in the low-latitude ocean (Coxall et al., 2005; Lear et al., 2008) and the onset of the benthic $\delta^{18}O$ increase (Fig. 5). However, the temperature change at Gran Barranca reflects an apparently abrupt cooling and partial rebound within the longer-term trend (Galeotti et al., 2016; Lear et al., 2008) of Late Eocene to Early Oligocene cooling. We suggest the general synchrony of marine and terrestrial records indicates that terrestrial climate responded directly to falling global $pCO_2$. Broadly, this pattern of temperature change strengthens the idea that the first step in the benthic $\delta^{18}O$ record was primarily

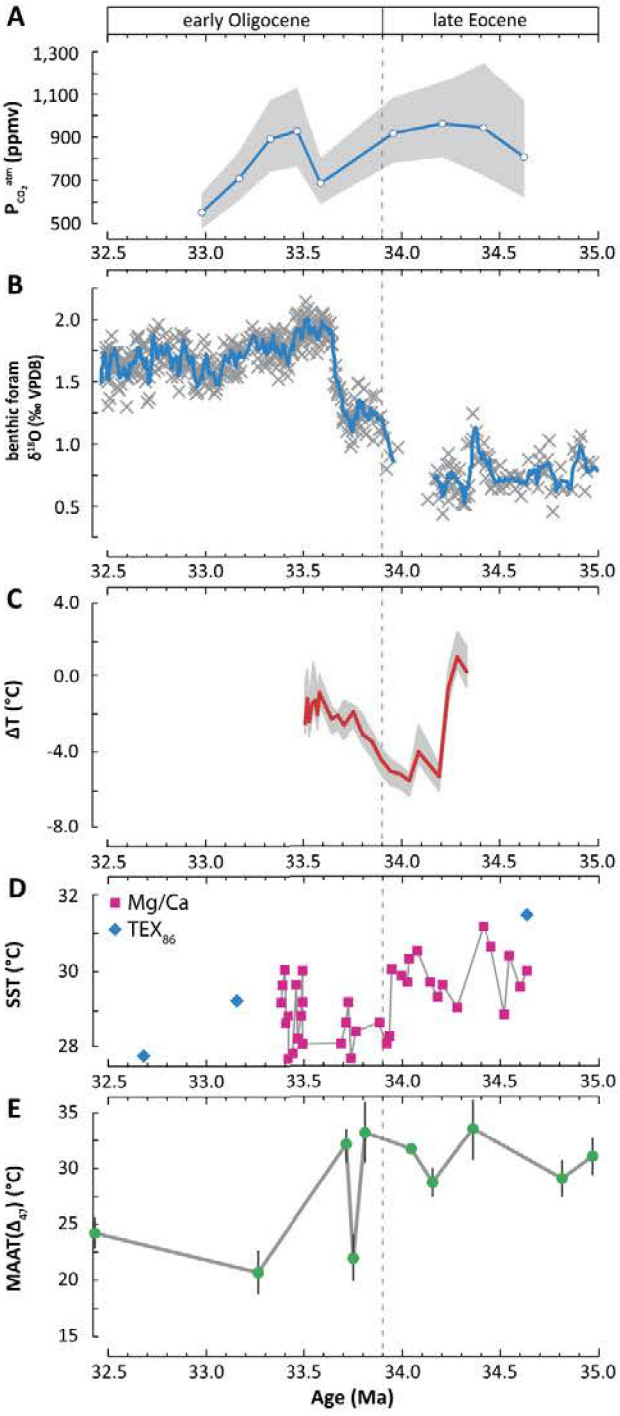


**Fig. 5.** Comparison of the terrestrial Patagonian EOT record to regional and global marine records of the EOT. (**A**) Marine $\delta^{11}B$-derived record of atmospheric $pCO_2$ (Pearson et al., 2009), replotted for changes in the $\delta^{11}B$ of seawater (Anagnostou et al., 2016). (**B**) Marine benthic foraminiferal calcite $\delta^{18}O$ record from ODP Site 1218 (Coxall et al., 2005). (**C**) Terrestrial temperature change from pre-EOT mean based on our $\delta D$ record from Patagonia, accounting for stepwise changes in ice volume (Bohaty et al., 2012). Error envelope reflects analytical and $\delta D$–$T$ relationship uncertainty. (**D**) Tropical SST record based on the Mg/Ca (Lear et al., 2008) and $TEX_{86}$ (Pearson et al., 2007) of well-preserved planktonic foraminifera from Tanzania. (**E**) Mid-latitude mean annual air temperature record based on carbonate clumped isotopes of freshwater gastropods from Hampshire Basin, UK (Hren et

smaller than temperature shifts observed at sites with substantial continentality (Fan et al., 2018; Zanazzi et al., 2007), which underscores the coherent response of the global climate system during the EOT.

The terrestrial cooling we observe is followed by a partial recovery. This rebound is truncated in the Vera Member by erosion or cessation of deposition, possibly in response to the newly established icehouse climate state. A similar return to warmer temperatures is also observed in foraminiferal Mg/Ca temperatures (Lear et al., 2008). The parallel nature of this terrestrial record with marine records suggests that the Gran Barranca record is an expression of a global event rather than a localized phenomenon. The simplest reason for this brief warming is the rebound in atmospheric $pCO_2$ (Pearson et al., 2009) (Fig. 5A), which is consistent with a transient pulse of warming prior to the establishment of cooler icehouse conditions and a stable ice sheet on Antarctica (Galeotti et al., 2016). This rebound in temperature explains why previous climate data from Gran Barranca (Kohn et al., 2004, 2015, 2010) had suggested negligible change across the EOT: we observe that the levels at which tooth enamel and soil carbonate nodules are available is located in a largely invariant part of our record that post-dates the recovery (Fig. 2).

The reconstructed temperature change during the EOT in Patagonia does not parallel metrics of regional biotic change—phytolith assemblages (Strömberg et al., 2013) and grazing mammal fauna (Reguero et al., 2010) change minimally during the EOT. In contrast to the significant extinctions documented in North American lineages of mammals, amphibians, reptiles, and both marine and terrestrial molluscs (Evanoff et al., 1992; Hutchison, 1992; Ivany et al., 2000) at the EOT, Patagonian flora and fauna appear unchanged. This generally indicates that factors other than temperature were important in driving biotic change in Patagonia. The abundance of burnt palm phytoliths varies through the time interval represented by the Vera Member (Selkin et al., 2015; see Fig. 2D), although it does not parallel reconstructed temperature change.

Phytoliths show little or no apparent ecosystem change across the EOT at Gran Barranca showing dominance by palms (*Arecaceae*) (Strömberg et al., 2013) prior to and after the EOT. Despite the persistence of this ecosystem indicator, extant palms tolerate a wide range of temperatures above MATs of 10 °C (Greenwood and Wing, 1995), and extend to ~40°S in South America in the present interglacial climate (Eiserhardt et al., 2011; Reichgelt et al., 2018). Reconstructed SST data from nearby DSDP Site 511 show minimum EOT MATs greater than 10–14 °C (Liu et al., 2009); thus palms likely remained viable in Patagonia during and following the EOT. The lack of apparent change in the floral community at the EOT could reflect the cosmopolitan nature of *Arecaceae* rather than a static climate. In short, precipitation stable isotopes and phytoliths record different environmental factors (temperature and vegetation change, respectively), but both records are consistent with changes in central Patagonia's climate during the EOT.

The current age model for the Vera Member (Dunn et al., 2013) indicates that our isotope data record cooling and an environmental response that is generally synchronous with records of the EOT from elsewhere on Earth. Alternative interpretation of paleomagnetic data (see discussion in Dunn et al., 2013) could place observed changes to stable isotope hydrology and cooling up to 1.3 Myr earlier, however a comparison of onshore (Gran Barranca) and South Atlantic offshore (ODP Site 511) data suggests a preference for the current depth-age model. These results demonstrate in atmospheric $pCO_2$ and regional ice buildup on Antarctica during this climate transition.

## 8. Conclusions

Terrestrial Patagonia cooled at the same time as the ocean at the onset of the EOT. Observed changes in stable isotope hydrology in Patagonia during this interval are consistent with GCM predictions of high latitude and Antarctic cooling and associated change in precipitation $\delta D$ across the EOT (Feakins et al., 2014). The rebound in Patagonian terrestrial temperature following initial cooling likely coincides with the transient resurgence of atmospheric $pCO_2$ at the EOGM (Pearson et al., 2009) and the initial expansion of ice on Antarctica (Galeotti et al., 2016). Though mechanisms for the transient rebound in atmospheric $pCO_2$ are debated (Zachos and Kump, 2005; Zachos et al., 1999) this increase in $pCO_2$ likely resulted in a near-return to pre-EOT conditions that is observed in both terrestrial and marine records (Lear et al., 2008). The correspondence between temperature change and atmospheric $pCO_2$ highlights the coupling of the ocean–atmosphere system in southern Patagonia and the role of $pCO_2$ in driving terrestrial climate change, particularly if changes in ocean circulation were responsible for the initial $pCO_2$ fall (Abelson and Erez, 2017; Elsworth et al., 2017).

## Acknowledgements

D.A.C. and M.T.H. designed research, D.A.C. performed research, D.A.C. and M.T.H. analyzed data, and D.A.C. and M.T.H. wrote the paper. This work was improved by discussions with Mark Pagani, Regan Dunn, Michael Henehan, Caroline Strömberg, and Srinath Krishnan. The manuscript benefitted from constructive reviews by Ilya Bindeman, Elizabeth Cassel, and two anonymous reviewers. We thank Antonia Beatrice Gilabert for local access and Andrea Piñones for help with planning. We acknowledge help in the field from Chelsea Colwyn and in the lab from Astrid Pacini. Support for this work was provided by NSF EAR-1650313 to Hren and by grants to Colwyn from the Geological Society of America, SEPM, AAPG, Yale Institute for Biospheric Studies, and the John F. Enders Fellowship.

## Appendix A. Supplementary material

Supplementary material related to this article can be found online at https://doi.org/10.1016/j.epsl.2019.01.052.

## References

Abelson, M., Erez, J., 2017. The onset of modern-like Atlantic meridional overturning circulation at the Eocene–Oligocene transition: evidence, causes, and possible implications for global cooling. Geochem. Geophys. Geosyst. 18, 2177–2199.

Ameghino, F., 1889. Contribucion al conocimiento de los mamiferos fosiles de la República Argentina: Obra escrita bajo los auspicios de la Academia nacional de ciencias de la República Argentina para ser presentada á la Exposicion universal de Paris de 1889. PE Coni é hijos.

Ameghino, F., 1906. Les formations sédimentaires du Crétacé supérieur et du Tertiaire de Patagonie. Imprenta de Juan A. Alsina.

Anagnostou, E., John, E.H., Edgar, K.M., Foster, G.L., Ridgwell, A., Inglis, G.N., Pancost, R.D., Lunt, D.J., Pearson, P.N., 2016. Changing atmospheric $CO_2$ concentration was the primary driver of early Cenozoic climate. Nature 533, 380–384.

Bellosi, E.S., 2010a. Loessic and fluvial sedimentation in Sarmiento Formation pyroclastics, middle Cenozoic of central Patagonia. In: Madden, R., Carlini, A., Vucetich, M.G., Kay, R. (Eds.), The Paleontology of Gran Barranca: Evolution and Environmental Change Through the Middle Cenozoic of Patagonia. Cambridge University Press, pp. 278–292.

Bellosi, E.S., Gonzalez, M.G., 2010. Paleosols of the middle Cenozoic Sarmiento Formation, central Patagonia. In: Madden, R., Carlini, A., Vucetich, M.G., Kay, R. (Eds.), The Paleontology of Gran Barranca: Evolution and Environmental Change Through the Middle Cenozoic of Patagonia. Cambridge University Press, pp. 293–305.

Bohaty, S.M., Zachos, J.C., Delaney, M.L., 2012. Foraminiferal Mg/Ca evidence for southern ocean cooling across the Eocene–Oligocene transition. Earth Planet. Sci. Lett. 317, 251–261.

Bowen, G.J., Revenaugh, J., 2003. Interpolating the isotopic composition of modern meteoric precipitation. Water Resour. Res. 39.

Bowen, G.J., Wilkinson, B., 2002. Spatial distribution of $\delta^{18}O$ in meteoric precipitation. Geology 30, 315–318.

Cassel, E.J., Breecker, D.O., 2017. Long-term stability of hydrogen isotope ratios in hydrated volcanic glass. Geochim. Cosmochim. Acta 200, 67–86.

Cassel, E.J., Graham, S.A., Chamberlain, C.P., 2009. Cenozoic tectonic and topographic evolution of the northern Sierra Nevada, California, through stable isotope paleoaltimetry in volcanic glass. Geology 37, 547–550.

Castro, J.M., Bindeman, I.N., Tuffen, H., Schipper, C.I., 2014. Explosive origin of silicic lava: textural and $\delta D$–$H_2O$ evidence for pyroclastic degassing during rhyolite effusion. Earth Planet. Sci. Lett. 405, 52–61.

Cerling, T.E., Brown, F.H., Bowman, J.R., 1985. Low-temperature alteration of volcanic glass: hydration, Na, K, $^{18}O$ and Ar mobility. Chem. Geol. 52, 281–293.

Channell, J., Galeotti, S., Martin, E.E., Billups, K., Scher, H., Stoner, J., 2003. Eocene to Miocene magnetostratigraphy, biostratigraphy, and chemostratigraphy at ODP Site 1090 (sub-Antarctic South Atlantic). Geol. Soc. Am. Bull. 115, 607–623.

Charles, C., Rind, D., Jouzel, J., Koster, R., Fairbanks, R., 1994. Glacial–interglacial changes in moisture sources for Greenland: influences on the ice core record of climate. Science 263, 508–511.

Coplen, T.B., Neiman, P.J., White, A.B., Landwehr, J.M., Ralph, F.M., Dettinger, M.D., 2008. Extreme changes in stable hydrogen isotopes and precipitation characteristics in a landfalling Pacific storm. Geophys. Res. Lett. 35.

Coxall, H.K., Wilson, P.A., Pälike, H., Lear, C.H., Backman, J., 2005. Rapid stepwise onset of Antarctic glaciation and deeper calcite compensation in the Pacific Ocean. Nature 433, 53–57.

Dansgaard, W., 1964. Stable isotopes in precipitation. Tellus 16, 436–468.

DeConto, R.M., Pollard, D., 2003. Rapid Cenozoic glaciation of Antarctica induced by declining atmospheric $CO_2$. Nature 421, 245–249.

Dettinger, M.P., Quade, J., 2015. Testing the analytical protocols and calibration of volcanic glass for the reconstruction of hydrogen isotopes in paleoprecipitation. In: Geological Society of America Memoirs, vol. 212, pp. 261–276.

Dunn, R.E., Madden, R.H., Kohn, M.J., Schmitz, M.D., Strömberg, C.A., Carlini, A.A., Ré, G.H., Crowley, J., 2013. A new chronology for middle Eocene–early Miocene South American Land Mammal Ages. Geol. Soc. Am. Bull. 125, 539–555.

Dunn, R.E., Strömberg, C.A., Madden, R.H., Kohn, M.J., Carlini, A.A., 2015. Linked canopy, climate, and faunal change in the Cenozoic of Patagonia. Science 347, 258–261.

Eiserhardt, W.L., Svenning, J.-C., Kissling, W.D., Balslev, H., 2011. Geographical ecology of the palms (Arecaceae): determinants of diversity and distributions across spatial scales. Ann. Bot. 108, 1391–1416.

Elsworth, G., Galbraith, E., Halverson, G., Yang, S., 2017. Enhanced weathering and $CO_2$ drawdown caused by latest Eocene strengthening of the Atlantic meridional overturning circulation. Nat. Geosci. 10, 213–216.

Evanoff, E., Prothero, D.R., Lander, R., 1992. Eocene–Oligocene climatic change in North America: the White River Formation near Douglas, east-central Wyoming. In: Eocene–Oligocene Biotic and Climatic Evolution. Princeton University Press, Princeton, New Jersey, pp. 116–130.

Fan, M., Ayyash, S.A., Tripati, A., Passey, B.H., Griffith, E.M., 2018. Terrestrial cooling and changes in hydroclimate in the continental interior of the United States across the Eocene–Oligocene boundary. Geol. Soc. Am. Bull. 130, 1073–1084.

Feakins, S.J., Warny, S., DeConto, R.M., 2014. Snapshot of cooling and drying before onset of Antarctic Glaciation. Earth Planet. Sci. Lett. 404, 154–166.

Fricke, H.C., O'Neil, J.R., 1999. The correlation between $^{18}O/^{16}O$ ratios of meteoric water and surface temperature: its use in investigating terrestrial climate change over geologic time. Earth Planet. Sci. Lett. 170, 181–196.

Friedman, I., Gleason, J., Sheppard, R.A., Gude, A.J., 1993a. Deuterium fractionation as water diffuses into silicic volcanic ash. Geophys. Monogr. 78, 321–323.

Friedman, I., Gleason, J., Warden, A., 1993b. Ancient climate from deuterium content of water in volcanic glass. Geophys. Monogr. 78, 309–319.

Friedman, I., Long, W., 1976. Hydration rate of obsidian. Science 191, 347–352.

Friedman, I., Long, W., 1984. Volcanic glasses, their origins and alteration processes. J. Non-Cryst. Solids 67, 127–133.

Friedman, I., Smith, R.L., 1958. The deuterium content of water in some volcanic glasses. Geochim. Cosmochim. Acta 15, 218–228.

Galeotti, S., DeConto, R., Naish, T., Stocchi, P., Florindo, F., Pagani, M., Barrett, P., Bohaty, S.M., Lanci, L., Pollard, D., 2016. Antarctic Ice Sheet variability across the

Gat, J.R., 1996. Oxygen and hydrogen isotopes in the hydrologic cycle. Annu. Rev. Earth Planet. Sci. 24, 225–262.

Goldner, A., Herold, N., Huber, M., 2014. Antarctic glaciation caused ocean circulation changes at the Eocene–Oligocene transition. Nature 511, 574–577.

Greenwood, D.R., Wing, S.L., 1995. Eocene continental climates and latitudinal temperature gradients. Geology 23, 1044–1048.

Hoke, G.D., Aranibar, J.N., Viale, M., Araneo, D.C., Llano, C., 2013. Seasonal moisture sources and the isotopic composition of precipitation, rivers, and carbonates across the Andes at 32.5–35.5°S. Geochem. Geophys. Geosyst. 14, 962–978.

Hren, M.T., Sheldon, N.D., Grimes, S.T., Collinson, M.E., Hooker, J.J., Bugler, M., Lohmann, K.C., 2013. Terrestrial cooling in Northern Europe during the Eocene–Oligocene transition. Proc. Natl. Acad. Sci. USA 110, 7562–7567.

Hutchison, J.H., 1992. Western North American reptile and amphibian record across the Eocene/Oligocene boundary and its climatic implications. In: Eocene–Oligocene Climatic and Biotic Evolution, 1051071962. 451–463.

Ivany, L.C., Patterson, W.P., Lohmann, K.C., 2000. Cooler winters as a possible cause of mass extinctions at the Eocene/Oligocene boundary. Nature 407, 887–890.

Jouzel, J., Alley, R.B., Cuffey, K., Dansgaard, W., Grootes, P., Hoffmann, G., Johnsen, S.J., Koster, R., Peel, D., Shuman, C., 1997. Validity of the temperature reconstruction from water isotopes in ice cores. J. Geophys. Res., Oceans 102, 26471–26487.

Kennett, J.P., 1977. Cenozoic evolution of Antarctic glaciation, the circum-Antarctic Ocean, and their impact on global paleoceanography. J. Geophys. Res. 82, 3843–3860.

Koffman, B., Kreutz, K., Breton, D., Kane, E., Winski, D., Birkel, S., Kurbatov, A., Handley, M., 2014. Centennial-scale variability of the Southern Hemisphere westerly wind belt in the eastern Pacific over the past millennium. Clim. Past 10, 1125–1144.

Kohn, M.J., Josef, J.A., Madden, R., Kay, R., Vucetich, G., Carlini, A.A., 2004. Climate stability across the Eocene–Oligocene transition, southern Argentina. Geology 32, 621–624.

Kohn, M.J., Strömberg, C.A., Madden, R.H., Dunn, R.E., Evans, S., Palacios, A., Carlini, A.A., 2015. Quasi-static Eocene–Oligocene climate in Patagonia promotes slow faunal evolution and mid-Cenozoic global cooling. Palaeogeogr. Palaeoclimatol. Palaeoecol. 435, 24–37.

Kohn, M.J., Zanazzi, A., Josef, J.A., 2010. Stable isotopes of fossil teeth and bones at Gran Barranca as monitors of climate change and tectonics. In: Madden, R., Carlini, A., Vucetich, M.G., Kay, R. (Eds.), The Paleontology of Gran Barranca: Evolution and Environmental Change Through the Middle Cenozoic of Patagonia. Cambridge University Press, New York, pp. 341–361.

Korasidis, V.A., Wallace, M.W., Wagstaff, B.E., Hill, R.S., 2018. Terrestrial cooling record through the Eocene–Oligocene transition of Australia. Glob. Planet. Change 173, 61–72.

Lamy, F., Hebbeln, D., Röhl, U., Wefer, G., 2001. Holocene rainfall variability in southern Chile: a marine record of latitudinal shifts of the Southern Westerlies. Earth Planet. Sci. Lett. 185, 369–382.

Lear, C.H., Bailey, T.R., Pearson, P.N., Coxall, H.K., Rosenthal, Y., 2008. Cooling and ice growth across the Eocene–Oligocene transition. Geology 36, 251–254.

Liu, Z., Bowen, G.J., Welker, J.M., 2010. Atmospheric circulation is reflected in precipitation isotope gradients over the conterminous United States. J. Geophys. Res., Atmos. (1984–2012) 115.

Liu, Z., Pagani, M., Zinniker, D., DeConto, R., Huber, M., Brinkhuis, H., Shah, S.R., Leckie, R.M., Pearson, A., 2009. Global cooling during the Eocene–Oligocene climate transition. Science 323, 1187–1190.

Madden, R.H., Kay, R.F., Guiomar, M., 2010. Gran Barranca: a 23-million-year record of middle Cenozoic faunal evolution in Patagonia. In: Madden, R., Carlini, A., Vucetich, M.G., Kay, R. (Eds.), The Paleontology of Gran Barranca: Evolution and Environmental Change Through the Middle Cenozoic of Patagonia. Cambridge University Press, New York, pp. 423–439.

Martin, E., Bindeman, I., Balan, E., Palandri, J., Seligman, A., Villemant, B., 2017. Hydrogen isotope determination by TC/EA technique in application to volcanic glass as a window into secondary hydration. J. Volcanol. Geotherm. Res. 348, 49–61.

Moy, C.M., Dunbar, R.B., Moreno, P.I., Francois, J.-P., Villa-Martínez, R., Mucciarone, D.M., Guilderson, T.P., Garreaud, R.D., 2008. Isotopic evidence for hydrologic change related to the westerlies in SW Patagonia, Chile, during the last millennium. Quat. Sci. Rev. 27, 1335–1349.

Pagani, M., Zachos, J.C., Freeman, K.H., Tipple, B., Bohaty, S., 2005. Marked decline in atmospheric carbon dioxide concentrations during the Paleogene. Science 309, 600–603.

Parrish, J.T., Ziegler, A., Scotese, C.R., 1982. Rainfall patterns and the distribution of coals and evaporites in the Mesozoic and Cenozoic. Palaeogeogr. Palaeoclimatol. Palaeoecol. 40, 67–101.

Pierrehumbert, R., 1999. Huascaran $\delta^{18}O$ as an indicator of tropical climate during the Last Glacial Maximum. Geophys. Res. Lett. 26, 1345–1348.

Poage, M.A., Chamberlain, C.P., 2001. Empirical relationships between elevation and the stable isotope composition of precipitation and surface waters: considerations for studies of paleoelevation change. Am. J. Sci. 301, 1–15.

Porter, T.J., Froese, D.G., Feakins, S.J., Bindeman, I.N., Mahony, M.E., Pautler, B.G., Reichart, G.-J., Sanborn, P.T., Simpson, M.J., Weijers, J.W., 2016. Multiple water isotope proxy reconstruction of extremely low last glacial temperatures in Eastern Beringia (Western Arctic). Quat. Sci. Rev. 137, 113–125.

Rapela, C., Spalletti, L., Merodio, J., Aragón, E., 1988. Temporal evolution and spatial variation of early Tertiary volcanism in the Patagonian Andes (40°S–42°30′S). J. South Am. Earth Sci. 1, 75–88.

Ré, G.H., Bellosi, E.S., Heizler, M., Vilas, J.F., Madden, R.H., Carlini, A.A., Kay, R.F., Vucetich, M.G., 2010a. A geochronology for the Sarmiento Formation at Gran Barranca. In: Madden, R., Carlini, A., Vucetich, M.G., Kay, R. (Eds.), The Paleontology of Gran Barranca: Evolution and Environmental Change Through the Middle Cenozoic of Patagonia. Cambridge University Press, New York, pp. 46–58.

Ré, G.H., Geuna, S.E., Vilas, J.F., Madden, R., Carlini, A., Vucetich, M., Kay, R., 2010b. Paleomagnetism and magnetostratigraphy of Sarmiento Formation (Eocene–Miocene) at Gran Barranca, Chubut, Argentina. In: Madden, R., Carlini, A., Vucetich, M.G., Kay, R. (Eds.), The Paleontology of Gran Barranca: Evolution and Environmental Change Through the Middle Cenozoic of Patagonia. Cambridge University Press, New York, pp. 32–45.

Reguero, M.A., Candela, A.M., Cassini, G.H., 2010. Hypsodonty and body size in rodent-like notoungulates. In: The Paleontology of Gran Barranca: Evolution and Environmental Change Through the Middle Cenozoic of Patagonia, p. 362.

Reichgelt, T., West, C.K., Greenwood, D.R., 2018. The relation between global palm distribution and climate. Sci. Rep. 8, 4721.

Ross, C., Smith, R., 1955. Water and other volatiles in volcanic glasses. Am. Mineral. 40, 1071–1089.

Rozanski, K., Araguás-Araguás, L., Gonfiantini, R., 1993. Isotopic patterns in modern global precipitation. In: Swart, P.K., Lohmann, K.C., McKenzie, J.A., Savin, S.M. (Eds.), Climate Change in Continental Isotopic Records. American Geophysical Union, pp. 1–36.

Scher, H.D., Bohaty, S.M., Zachos, J.C., Delaney, M.L., 2011. Two-stepping into the icehouse: east Antarctic weathering during progressive ice-sheet expansion at the Eocene–Oligocene transition. Geology 39, 383–386.

Schmidt, G.A., LeGrande, A.N., Hoffmann, G., 2007. Water isotope expressions of intrinsic and forced variability in a coupled ocean–atmosphere model. J. Geophys. Res., Atmos. 112.

Schneider, T., 2006. The general circulation of the atmosphere. Annu. Rev. Earth Planet. Sci. 34, 655–688.

Secord, R., Gingerich, P.D., Lohmann, K.C., MacLeod, K.G., 2010. Continental warming preceding the Palaeocene–Eocene thermal maximum. Nature 467, 955–958.

Seligman, A.N., Bindeman, I.N., Watkins, J.M., Ross, A.M., 2016. Water in volcanic glass: from volcanic degassing to secondary hydration. Geochim. Cosmochim. Acta 191, 216–238.

Selkin, P.A., Strömberg, C.A., Dunn, R., Kohn, M.J., Carlini, A.A., Davies-Vollum, S., Madden, R.H., 2015. Climate, dust, and fire across the Eocene–Oligocene transition, Patagonia. Geology, G36664. 36661.

Seton, M., Müller, R., Zahirovic, S., Gaina, C., Torsvik, T., Shephard, G., Talsma, A., Gurnis, M., Turner, M., Maus, S., 2012. Global continental and ocean basin reconstructions since 200 Ma. Earth-Sci. Rev. 113, 212–270.

Sheldon, N.D., 2009. Nonmarine records of climatic change across the Eocene–Oligocene transition. Spec. Pap., Geol. Soc. Am. 452, 241–248.

Sheldon, N.D., Costa, E., Cabrera, L., Garces, M., 2012. Continental climatic and weathering response to the Eocene–Oligocene transition. J. Geol. 120, 227–236.

Sheldon, N.D., Grimes, S.T., Hooker, J.J., Collinson, M.E., Bugler, M.J., Hren, M.T., Price, G.D., Sutton, P.A., 2016. Coupling of marine and continental oxygen isotope records during the Eocene–Oligocene transition. Geol. Soc. Am. Bull. 128, 502–510.

Simpson, G.G., 1930. Scarritt–Patagonian Expedition Field Notes. American Museum of Natural History, New York. Available at http://paleo.amnh.org/notebooks/index.html.

Smith, R.B., Evans, J.P., 2007. Orographic precipitation and water vapor fractionation over the southern Andes. J. Hydrometeorol. 8, 3–19.

Stern, L.A., Blisniuk, P.M., 2002. Stable isotope composition of precipitation across the southern Patagonian Andes. J. Geophys. Res. 107, 4667.

Strömberg, C.A., Dunn, R.E., Madden, R.H., Kohn, M.J., Carlini, A.A., 2013. Decoupling the spread of grasslands from the evolution of grazer-type herbivores in South America. Nat. Commun. 4, 1478.

Terry, D.O., 2001. Paleopedology of the Chadron Formation of Northwestern Nebraska: implications for paleoclimatic change in the North American midcontinent across the Eocene–Oligocene boundary. Palaeogeogr. Palaeoclimatol. Palaeoecol. 168, 1–38.

Williams, G.P., 1988. The dynamical range of global circulations—I. Clim. Dyn. 2, 205–260.

Zachos, J.C., Kump, L.R., 2005. Carbon cycle feedbacks and the initiation of Antarctic glaciation in the earliest Oligocene. Glob. Planet. Change 47, 51–66.

Zachos, J.C., Opdyke, B.N., Quinn, T.M., Jones, C.E., Halliday, A.N., 1999. Early Cenozoic glaciation, Antarctic weathering, and seawater $^{87}Sr/^{86}Sr$: is there a link? Chem. Geol. 161, 165–180.

Zachos, J., Pagani, M., Sloan, L., Thomas, E., Billups, K., 2001. Trends, rhythms, and aberrations in global climate 65 Ma to present. Science 292, 686–693.

Zanazzi, A., Kohn, M.J., MacFadden, B.J., Terry, D.O., 2007. Large temperature drop across the Eocene–Oligocene transition in central North America. Nature 445, 639–642.

Zhang, Y.G., Pagani, M., Liu, Z., Bohaty, S.M., DeConto, R., 2013. A 40-million-year history of atmospheric $CO_2$. Philos. Trans. R. Soc. A 371, 20130096.